Progress in Physics of Applied Materials 5 (2025), 83 – 93

Semnan University

Progress in Physics of Applied Materials

journal homepage: https://ppam.semnan.ac.ir/

First-Principles Investigation of Erbium Doping and Intrinsic Defects on the Structural and Electronic Properties of Silicon Dioxide

Joshua Adeyemi Owolabi [a*], Haruna Ali [a], Mohammed Yusuf Onimisi [a], Benedict Machu [a], Alhassan Shuaibu [b], Isaac Hyuk Daniel [b], Mary Samuel [c], Olalekan Joel Awujoola [d]

[a] *Department of Physics, Nigerian Defence Academy, Kaduna, Nigeria*
[b] *Department of Physics, Kaduna State University, Kaduna, Nigeria*
[c] *Department of Mechanical Engineering Nigerian Defence Academy, Kaduna, Nigeria*
[d] *Department of Computer Science, Nigerian Defence Academy, Kaduna*

ARTICLE INFO

Article history:
Received: 31 March 2025
Revised: 3 July 2025
Accepted: 12 July 2025
Published online: 29 July 2025

Keywords:
Erbium Doping;
Silica Nanostructures;
DFT-GGA;
Band Gap;
Intrinsic Defects;
Optoelectronics.

ABSTRACT

Rare-earth-doped silica (SiO_2) nanostructures have great potential for optoelectronics but little is known about the atomic-scale processes controlling their electrical behaviour in the presence of intrinsic defects and erbium (Er) doping. In order to close this gap, this work uses the Density Functional Theory with Generalized Gradient Approximation (DFT-GGA), a first-principles density functional theory, to analyse the structural and electrical changes in Er-doped SiO_2 and its defective forms. Er was used to replace Si atoms in three doping concentration models of 2.08%, 4.17%, and 6.25%, for silicon vacancies (SiV) and oxygen vacancies (OV), which were added to evaluate defect-mediated effects. Lattice expansion proportionate to Er concentration was found by structural optimisation, which was driven by Er–O bonds of 2.1 – 2.3 Å and larger ionic radius 2.45 Å and 1.46 Å for Si. Thermodynamic stability was demonstrated by formation energies ranging from -0.675 to -0.724 eV/atom, where lower energy configurations were preferred by increased Er content. Er 4f, which derives the impurity states near the conduction band, is responsible for the transition to a direct band gap. The band structure calculations show moderate Er doping at 4.17%, which shows SiO_2's indirect band gap of 5.32 eV to the doped indirect band gap of 5.98 eV and direct band gap of 5.01 and 5.08 eV. Due to dopant interactions changing of the host matrix, the gap unexpectedly extended to 5.89 eV at 6.25% Er concentration. Oxygen and silicon vacancies further modulated electronic properties, introducing deep donor levels and reducing the gap of O_V to 3.89 eV and Si_V to 4.21 eV formation energy albeit at significant energetic costs. Density of states analysis highlighted hybridization between Er 4f and 5d orbitals and host O 2p and Si 3p states, enabling tailored band engineering. This work establishes a theoretical framework linking Er doping and defects to tunable electronic properties in SiO_2, offering insights for designing high-efficiency optoelectronic materials.

1. Introduction

Rare-earth (RE) ion integration into semiconductor matrices has transformed optoelectronics, with Erbium (Er)-doped silica (SiO_2) nanostructures emerging as key components in applications such as environmental remediation, photovoltaic, and telecommunications [1–3]. Silica's intrinsic properties of wide bandgap, high exciton binding energy, and chemical inertness make it an ideal host for optically active RE dopants, enabling efficient exciton-mediated luminescence which forms the foundation of next-generation optoelectronic devices [4–6]. Erbium, in

---

* Corresponding author. Tel.: +98-234-7031699937
E-mail address: jaowolabi@nda.edu.ng

Cite this article as:
Owolabi J.A., Ali H., Onimisi M.S., Machu B., Shuaibu A., Daniel I.H., Samuel M., and Awujoola O.J., 2025. First-Principles Investigation of Erbium Doping and Intrinsic Defects on the Structural and Electronic Properties of Silicon Dioxide. *Progress in Physics of Applied Materials*, *5*(2), pp.83-93. DOI: **10.22075/PPAM.2025.37283.1142**

particular, is of great interest due to its intra-4f electronic transitions, which allow for efficient infrared to visible light conversion and emission at the telecommunication critical wavelength of 1.54 µm [7, 8].

Recent experimental advances continue to demonstrate the versatility of Er and SiO_2, for instance, Hernández et al. in 2024 reported a 40% enhancement in up conversion photoluminescence using sol–gel derived for Er and SiO_2 [9], while Ledakowicz and Paździor in 2021 achieved complete photocatalytic degradation of DR-31 dye under UV light by optimizing Er concentration [10]. In addition, Er–SiO_2's dielectric properties make it suitable for high-frequency electronics such as 5G and 6G technologies [3].

Despite these developments, the atomic-scale understanding of the structural and electronic effects of Er doping in SiO_2 remains limited. While theoretical models have been applied to similar doped systems such as La- and Ce-doped silica [11] and oxygen deficient SiO_2 under radiation exposure [12], the unique dopant-defect interplay in Er-doped SiO_2 is largely unexamined. For instance, Chen et al., in 2023 demonstrated that ultrafast laser-induced silicon vacancies reduce the bandgap of SiO_2 by 0.8 eV, revealing the critical impact of defects on optoelectronic performance [13]. Yet, theoretical frameworks for the combined effects of Er doping and intrinsic defects in SiO_2 remain inadequate [14].

To address this gap, this work employs first-principles Density Functional Theory (DFT) within the Generalized Gradient Approximation (GGA), as implemented in Quantum ESPRESSO, to systematically explore how Erbium doping concentration of 2.08%, 4.17%, and 6.25% affects the structural and electronic properties of SiO_2. Central to this methodology is solving the Kohn–Sham equations, which reformulate the many-body electron problem into a set of non-interacting single-particle equations as shown in equation 1:

$$\left[-\frac{\hbar^2}{2m}\nabla^2 + V_{eff}(r)\right]\psi_i(r) = \varepsilon_i \psi_i(r) \qquad (1)$$

Where $\psi_i(r)$ and ε_i are the Kohn-Sham orbitals and energies, respectively, and $V_{eff}(r)$ includes the external potential, the Hartree potential, and the exchange–correlation potential $V_{XC}(r)$ approximation using the GGA functional. These equations are solved self-consistently using a plane wave basis set and norm-conserving and ultrasoft pseudopotentials.

In addition to total energy and geometry optimizations, the Density of States (DOS) and Projected Density of States (PDOS) are calculated to analyze changes in the electronic structure due to Er incorporation. The total DOS is defined as:

$$D(E) = \sum_i \delta(E - \varepsilon_i) \qquad (2)$$

Where ε_i are the Kohn–Sham eigenvalues, and the Dirac delta function δ is typically broadened using a Gaussian function for numerical integration. The PDOS further resolves the contribution of specific atomic orbitals of Er 4f and O 2p to the electronic states, and is given by:

$$D_\alpha(E) = \sum_i \left|\langle \varphi_\alpha | \psi_i \rangle\right|^2 \delta(E - \varepsilon_i) \qquad (3)$$

Where ϕ_α is an atomic-like orbital centered on atom α, and $\left|\langle \phi_\alpha | \psi_i \rangle\right|^2$ represents the orbital weight of state i on atom α. This decomposition provides critical insight into orbital hybridization of Er 4f and O 2p interactions, impurity levels, and defect-related states within the bandgap.

By leveraging on these methods, this study quantifies the local lattice distortions caused by the larger ionic radius of Er^{3+} at 2.45 Å compared to Si^{4+} at 1.46 Å, and correlates them with changes in lattice constants, formation energies, and bonding characteristics. Further, PDOS analysis reveals how Er doping introduces impurity bands, narrows the bandgap, and potentially modifies carrier recombination mechanisms, all of which are essential for tailoring the optical and electronic performance of Er–SiO_2 systems.

Thus, this work provides a foundational theoretical understanding of Er-doped SiO_2 by linking quantum-level interactions to macroscopic material behavior, enabling defect and dopant aware design for future optoelectronic and photonic technologies.

2. Model Description and Computational Method

2.1. Model Description

Figure 1, shows how the characterized crystal structure was chosen as the host material in the crystal structure selection process where pure SiO_2 was selected as the host material.

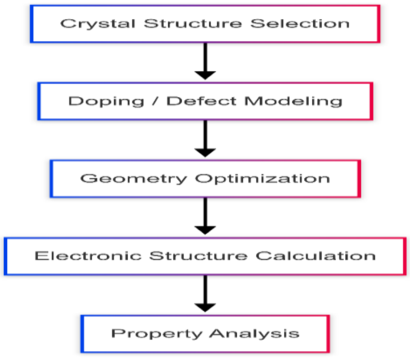

Fig. 1. workflow model of doping and intrinsic point defects in pure silicon dioxide (SiO_2)

The crystal structure is 4/mmm symmetric and belongs to the $P4_2/mbc$ space group. The lattice parameters and atomic locations, were gathered from the Materials Project database before the structural data were calculated. There are sixteen silicon atoms and thirty-two oxygen atoms in the basic unit cell of pure SiO_2. To examine the effects, controlled alterations were made to the pristine SiO_2 structure in the doping and defect area.

In order to replicate Erbium (Er) doping, Erbium atoms were substituted for one, two, and three silicon atoms. As a result, doping concentrations of 2.08%, 4.17%, and 6.25% were used for the computation, respectively. One silicon atom was taken out of the optimized SiO_2 structure to imitate a silicon vacancy (SiV), while one oxygen atom was taken out to construct an oxygen vacancy (OV) for the intrinsic point defects.

The modified structures' lowest energy configurations were attained by optimizing their geometry. After doping, geometry optimization was applied to the structures. This stage ensures that any distortions caused by the added dopants and vacancies are taken into account as the system relaxes into a stable configuration.

The optimization process adjusts the atomic positions, lattice parameters, and other structural parameters to minimize the total energy of the system. During the electronic structure calculation, Density Functional Theory (DFT) was used to calculate the optimized structures' electronic characteristics. The band structure was also obtained, and it identifies doping-induced alterations as well as the electronic bandgap.

Additionally, the Density of States (DOS) was obtained in order to examine the distribution of electronic states and comprehend the impact of vacancy and doping on the electronic density.

These calculations provide insights into the electronic behavior of the doped and defective SiO_2 systems. The property analyzed the physical and optical properties of the modified SiO_2 structures based on the results from the electronic structure calculations.

2.2. Computational Method

All calculations were carried out using DFT as implemented in the Quantum ESPRESSO package [6]. The Generalized Gradient Approximation (GGA) with the Perdew–Burke–Ernzerhof (PBE) exchange-correlation functional [15] was employed to account for electron interaction effects. The interactions between valence electrons and ionic cores were described using the ultrasoft pseudopotential method. The valence electron configurations used in the calculations are Si: $2p^6\ 3s^2\ 3p^2$, O: $2s^2\ 2p^4$, and Er: $4f^{12}\ 5s^2\ 5p^6\ 6s^2$, while Structural relaxations were performed using the Broyden–Fletcher–Goldfarb–Shanno (BFGS) algorithm to minimize the total energy of the system. The plane-wave cutoff energy was set to 40 Ry (544.22649 eV) for all calculations. The Brillouin zone integration was performed using the Monkhorst–Pack k-point sampling of 5×5×5 grid for pure SiO_2 and 4×4×4 grid for Er-doped configurations. The self-consistent field (SCF) cycles converged when the total energy change was less than 10^{-5} eV per atom. Subsequently, the systems underwent full structural relaxation, with convergence criteria including a maximum force on each atom below 0.03 eV/Å, internal stress under 0.05 GPa, and atomic displacements less than 0.01 Å. A summary of the key computational parameters is presented in Table 1 for clarity and reproducibility.

Table 1. Computational Parameters

Parameter	**Value / Description**
Software Package	Quantum ESPRESSO
DFT Functional	GGA-PBE
Pseudopotentials	Ultrasoft pseudopotentials
Plane-Wave Cutoff Energy	40 Ry (544.22649 eV)
k-Point Grid (pure SiO_2)	5×5×5
k-Point Grid (Er-doped SiO_2)	4×4×4
Convergence Threshold (SCF)	10^{-5} eV/atom
Force Convergence Criterion	< 0.03 eV/Å
Stress Convergence Criterion	< 0.05 GPa
Max Atomic Displacement	< 0.01 Å
Valence Configurations	Si: $2p^6\ 3s^2\ 3p^2$; O: $2s^2\ 2p^4$; Er: $4f^{12}\ 5s^2\ 5p^6\ 6s^2$

3. Results and Discussion

3.1. Optimization of Crystal Structures

The optimized crystal structures of pure silicon dioxide and Erbium (Er) doped SiO_2 at different doping concentration levels are shown in Figure 2. Panel (a) of Figure 2 shows pure SiO_2, while panels (b), (c), and (d) represent the structures after replacing one, two, and three Si atoms with Er atoms, suited for doping concentration levels of 2.08%, 4.17%, and 6.25%, respectively. Silicon (Si) atoms are shown for every subfigure as tan sphere, oxygen (O) atoms in red, and Erbium (Er) impurities in green. More green spheres replace Si atoms as the Er concentration increases from panel (b) to panel (d), thereby causing more local deformation around the Er sites. The structural, energetic, and electronic analysis of Er-doped SiO_2 presented in this study reveals several notable trends with increasing Er concentration. Structurally, as illustrated in Figure 2 and Table 2, both the lattice parameters and the unit cell volume increase systematically with rising Er content. This is primarily due to the larger ionic radius of Er^{3+} at 2.45 Å compared to that of Si^{4+} at 1.46 Å, which leads to local lattice distortion and global expansion. The bond length analysis confirms this, showing that Er–O bonds are significantly longer than Si–O bonds, introducing localized strain fields around dopant sites.

Table 2 elucidates the effects of Erbium (Er) doping on the structural, energetic, and electronic properties of silicon dioxide (SiO_2). By analyzing variations in cell parameters, formation energy, bond lengths, and Mulliken charges across different Er concentrations, we gain insights into the modifications induced in the SiO_2 matrix. In pure SiO_2, the lattice parameters are a = 9.905 Å and c = 8.478 Å, resulting in a unit cell volume of 831.739 Å^3. Upon doping with Er, these parameters exhibit a gradual increase for $Si_{0.9717}Er_{0.0208}O_2$, a = 9.955 Å and c = 8.498 Å with a volume of 831.789 Å^3; for $Si_{0.9583}Er_{0.0417}O_2$, a = 9.995 Å and c = 8.528 Å with a volume of 831.839 Å^3; and for $Si_{0.9375}Er_{0.0625}O_2$, a = 10.015 Å and c = 8.568 Å with a volume of 831.899 Å^3.

This expansion is attributed to the larger ionic radius of Er^{3+} compared to Si^{4+}, leading to an overall increase in unit cell volume. Such structural alterations can influence the material's mechanical and thermal properties, potentially enhancing its applicability in various technological domains such as optical communication, integrated photonics, medical applications, quantum technology, and glass manufacturing. The formation energy per atom becomes more negative with increasing Er concentration, indicating enhanced thermodynamic stability of the doped structures. Specifically, pure SiO_2 has a formation energy of -0.552 eV/atom while $Si_{0.9717}Er_{0.0208}O_2$, has -0.675 eV/atom, $Si_{0.9583}Er_{0.0417}O_2$, has -0.699 eV/atom; and $Si_{0.9375}Er_{0.0625}O_2$, for -0.724 eV/atom.

The formation energy ($E_{(form)}$) is computed using equation 4:

$$E_{(form)} = E_{(Si_{1-x}Er_xO_2)} + E_{(SiO_2)} + (\mu_{(Si)} + \mu_{(Er)}) \qquad (4)$$

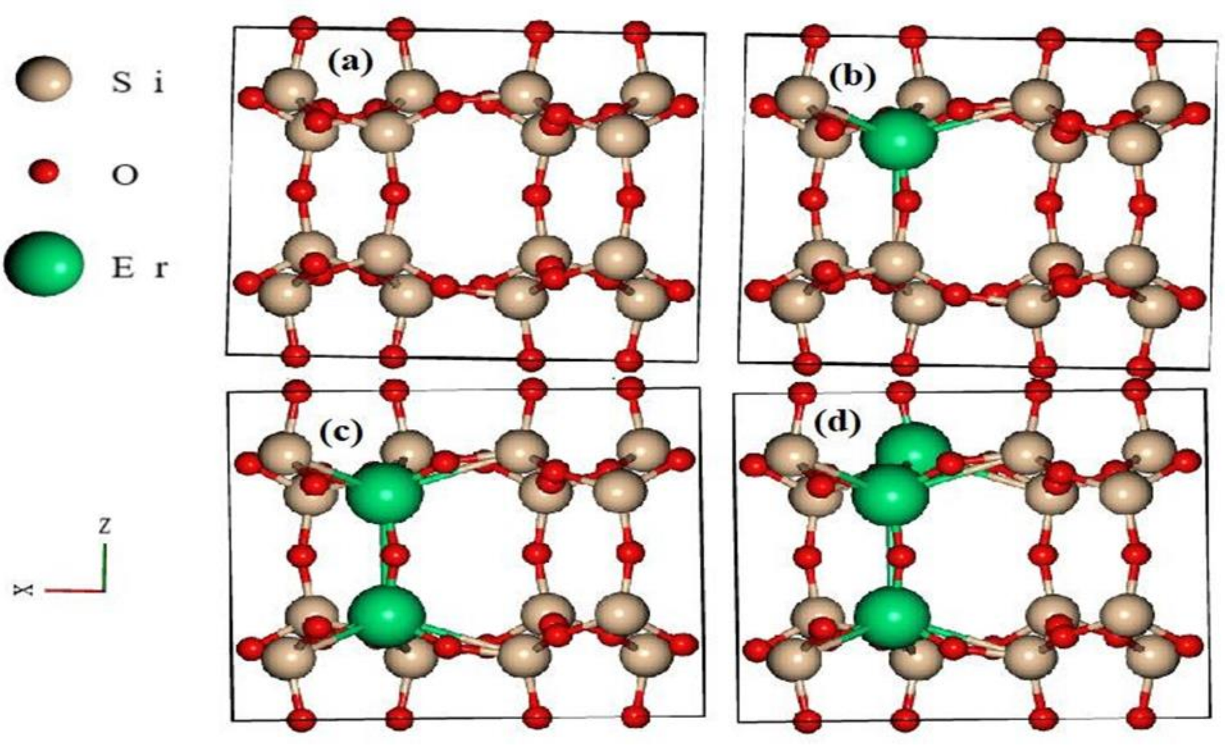

Fig. 2. The optimized structure of (a) pure SiO_2, (b) $Si_{0.9717}Er_{\ 0.0283}O_2$, (c) $Si_{0.9583}Er_{\ 0.0417}O_2$, and (d) $Si_{0.9375}Er_{\ 0.0625}O_2$

Table 2. Calculated cell parameters, volume, formation energy ($Eform$), bond lengths, and Mulliken charges of pure SiO_2, and SiO_2 doped with various Er concentrations

	Cell parameters		**Volume (Å^3)**	E_{form} eV/atom	**Bond length (Å)**		**Mulliken charges**		
	a(Å)	***c***(Å)			**Si-O**	**Er-O**	**Si**	**Er**	**O**
Pure SiO_2	9.905	8.478	831.739	-0.552	1.611	-	1.28	1.54	-1.09
$Si_{0.9717}Er_{0.0208}O_2$	9.955	8.498	831.789	-0.675	1.663	2.31116	1.32	1.58	-1.00
$Si_{0.9583}Er_{0.0417}O_2$	9.995	8.528	831.839	-0.699	1.699	2.22117	1.30	1.61	-1.00
$Si_{0.9375}Er_{0.0625}O_2$	10.015	8.568	831.899	-0.724	1.712	2.11103	1.38	1.62	-1.00
Experimental value [16]	-	-	-	-	-	~2.27 Å at 3%, ~2.29 Å at 6 %	-	-	-
Combined Experimental & Theoretical value [17]	-	--	-	-	-	~2.2–2.3 Å 2.2–2.3 Å	-	-	-

where $E_{(}SiO_{2)}$ is the energy of the pristine host material and $E_{(}Si_{1-x}Er_xO_{2)}$ is the energy of the doped system at 2.08%, 4.17%, and 6.25%, concentration, $\mu_{(}Si_{)}$ and $\mu_{(}Er_{)}$ are the chemical potentials of Si and Er, respectively. For Oxygen and Erbium under silicon rich circumstances, $\mu_{(}Si_{)}$ equals the energy of bulk Si while similar arguments hold. The doped systems are still energetically preferred and therefore probably fit for laboratory synthesis, though the negative formation energies imply that pure SiO_2 remains probably the most stable arrangement. This trend suggests that Er incorporation stabilizes the SiO_2 matrix, possibly due to favorable interactions between Er atoms and the surrounding oxygen atoms. Such findings align with previous studies where rare-earth doping has been shown to stabilize host matrices, thereby improving material performance in specific applications [2].

In examining the bond lengths, the Si–O bond length in pure SiO_2 is 1.611 Å. With increasing Er content, this bond length slightly increases from 1.663 Å in $Si_{0.9717}Er_{0.0208}O_2$, 1.699 Å in $Si_{0.9583}Er_{0.0417}O_2$, and 1.712 Å in $Si_{0.9375}Er_{0.0625}O_2$. Additionally, Er–O bond lengths are observed as 2.311 Å in $Si_{0.9717}Er_{0.0208}O_2$, 2.221 Å in $Si_{0.9583}Er_{0.0417}O_2$, and 2.111 Å in $Si_{0.9375}Er_{0.0625}O_2$. These longer Er–O bonds reflect the structural adjustments accommodating the larger Er ions. These changes in bond lengths can influence the vibrational properties of the material, potentially affecting its phonon dynamics and thermal conductivity [18].

Mulliken charge analysis reveals a redistribution of electronic charge upon Er doping. In pure SiO_2, the charges are Si: +1.28, O: -1.09. With Er doping, the charges become 1.54 while in $Si_{0.9717}Er_{0.0208}O_2$, Si: +1.32, Er: +1.58, O: -1.00; in $Si_{0.9583}Er_{0.0417}O_2$, Si: +1.30, Er: +1.61, O: -1.00; and in $Si_{0.9375}Er_{0.0625}O_2$, Si: +1.38, Er: +1.62, O: -1.00. The slight increase in positive charge on Si atoms and the consistent negative charge on oxygen atoms suggest a rebalancing of charge to accommodate the trivalent Er ions. This charge redistribution can influence the electronic structure, potentially modify the band gap, and affect the material's optical absorption and emission characteristics.

The incorporation of Er into SiO_2 has significant implications for photonic and optoelectronic applications. Erbium-doped materials are renowned for their luminescence at 1.54 µm, a wavelength crucial for optical communication technologies. The structural and electronic modifications observed in the doped SiO_2 suggest potential enhancements in luminescent efficiency and stability, making these materials promising candidates for fiber amplifiers, lasers, and integrated photonic devices.

Previous research has demonstrated the benefits of rare-earth doping in various host matrices, leading to improved optical and electronic properties. For instance, studies on Er-doped glass systems have reported enhanced luminescence and stability, corroborating the findings in the current study. While the study provides valuable insights into the effects of Er doping in SiO_2, it primarily focuses on structural and electronic properties. Further investigations into the optical behavior, such as photoluminescence efficiency and lifetime measurements, would offer a more comprehensive understanding of the material's suitability for photonic applications. Additionally, exploring the effects of varying doping concentrations beyond the studied range could reveal optimal doping levels for desired properties.

To build upon the current findings, future research could explore optical characterization by investigating the photoluminescence properties of Er-doped SiO_2 to assess its efficacy in optical applications. Examining the thermal behavior of the doped materials to ensure stability under operational conditions would also be beneficial. Developing and testing devices incorporating Er-doped SiO_2 to evaluate performance in real-world applications would provide a holistic understanding of the material's capabilities and limitations, guiding its application in advanced technologies.

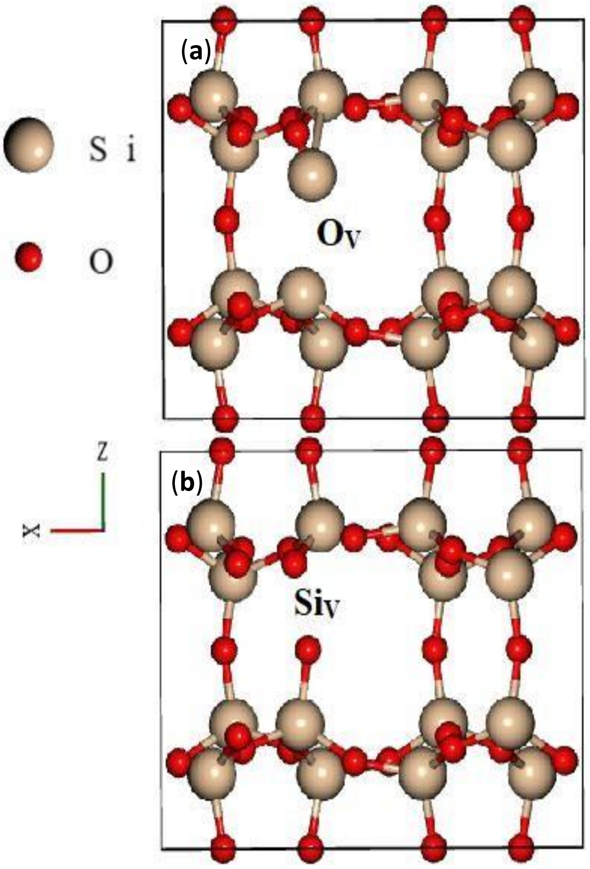

Fig. 3. Optimized structures of (a) SiO_2 +OV (b) SiO_2+SiV

Figure 3 illustrates the relaxed atomic configurations of SiO_2 containing intrinsic point defects in panel a and b. Panel (a) shows the structure with an oxygen vacancy (OV), while panel (b) displays the silicon vacancy (SiV). These defects were created by selectively removing a single O or Si atom from the lattice, followed by full geometry optimization. The images show noticeable local distortions near the vacancy sites, reflecting the disruption of the regular tetrahedral coordination typically observed in the pristine SiO_2 network. To quantitatively assess these structural changes and their energetic implications, Table 3 presents the computed lattice constants a and c, unit cell volumes, and defect formation energies ($E_{(}d/form_{)}$) for both OV and SiV. The formation energy of the vacancy is calculated using Equation 5:

$$E_{d/_{form}} = E_{defect} - (n \pm 1)E_{SiO_2} \qquad (5)$$

Table 3. Calculated cell parameters, volume, and vacancy formation energy of Er / SiO_2 with native defects (OV or SiV)

	Cell parameters		**Volume (Å³)**	$Ed/form$**(eV/atom)**	
	a(Å)	a(Å)		$(n+1)$	$(n-1)$
SiO_2+OV	9.8431	8.674	832.561	3.89	1.76
SiO_2+SiV	9.7224	8.844	841.232	4.21	1.97

In this expression, E_{defect} is the total energy of the SiO_2 supercell containing the vacancy, n is the number of atoms in the perfect supercell, and E_{SiO_2} is the energy per atom of the pristine structure. The (n−1) term is used when a vacancy is introduced, while (n+1) applies for interstitial defects. The presence of vacancies significantly alters the structural parameters. In both defects, the a-lattice constant contracts relative to pure SiO_2 from 9.905 Å in the pristine to 9.843 Å for OV and 9.722 Å for SiV, suggesting a localized inward relaxation around the vacancy sites. Conversely, the c-lattice parameter increases from 8.478 Å to 8.674 Å for OV and 8.844 Å for SiV, which, combined with rearranged bonding and results in an overall increase in cell volume to 832.561 Å^3 for OV and 841.232 Å^3 for SiV. These observations suggest anisotropic lattice distortion, possibly driven by the system's attempt to re-equilibrate bonding stresses introduced by atom removal.

In terms of energetics, the defects exhibit positive formation energies, indicating that they are energetically unfavorable under equilibrium conditions. The formation energy values, computed using both the n+1 and n−1 variants for comparison, show that, for the OV system, the formation energy is 3.89 eV/atom using n+1 and 1.76 eV/atom using n−1 while for the SiV system, the corresponding values are 4.21 eV/atom and 1.97 eV/atom, respectively.

The higher formation energy of SiV compared to OV implies that creating a silicon vacancy is more energetically costly than an oxygen vacancy, likely due to the central structural role that Si atoms play in the silica tetrahedral network. In both cases, however, the positive and relatively high defect formation energies underscore the thermodynamic preference for defect-free (pristine) SiO_2 and suggest that under standard synthesis conditions, significant external energy input would be required to create such defects.

3.2. Impact of Er Doping Concentration on the Electronic Properties of SiO_2

Figure 4 presents the calculated band structures of SiO_2 under increasing erbium (Er) doping concentrations, with all energies referenced to the Fermi level set at 0 eV.

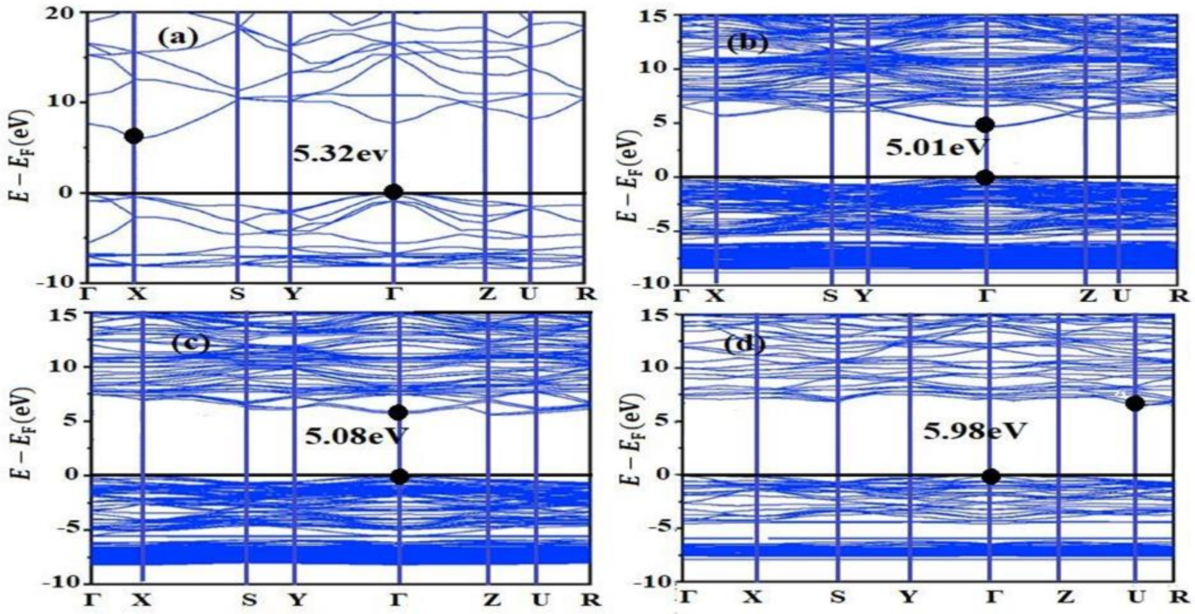

Fig. 4. Band structures of pure SiO_2 and SiO_2 doped systems, where the Fermi level is set to 0: (a) pure SiO_2, (b) $Si_{0.9717}Er_{0.0283}O_2$, (c) $Si_{0.9583}Er_{0.0417}O_2$, and (d) $Si_{0.9375}Er_{0.0625}O_2$

The panels show (a) pristine SiO_2, (b) $Si_{0.9717}Er_{0.0283}O_2$ (2.08% Er), (c) $Si_{0.9583}Er_{0.0417}O_2$ (4.17% Er), and (d) $Si_{0.9375}Er_{0.0625}O_2$ (6.25% Er).

Figure 4a shows pristine SiO_2, which exhibits a wide indirect band gap of approximately 5.32 eV, consistent with theoretical predictions using a GGA-based functional [7, 19-22]. While this value underestimates the experimental band gap of ~9.0 eV due to known DFT limitations, it provides a reliable baseline for tracking doping-induced changes. The conduction band minimum (CBM) and valence band maximum (VBM) are located at different k-points, affirming the indirect nature of the gap. When Er is substituted at 2.08% concentrations in Figure 4b and 4.17% in Figure 4c, significant changes in the band structure show the band gap narrows to 5.01 eV and 5.08 eV, respectively. The nature of the band gap transitions from indirect to direct, with both VBM and CBM now aligning at the same k-point.

This band gap narrowing and direct transition are attributable to the introduction of Er 4f-derived impurity states near the conduction band edge. The sp-f exchange interaction between Er's localized 4f electrons and the delocalized states of the SiO_2 matrix leads to a perturbation in the conduction band, effectively lowering the CBM. These new states act as shallow recombination centers, which enhance radiative recombination for a beneficial property for optoelectronic applications. In Figure 4d, as Er concentration increases to 6.25%, the band gap increases again to ~5.89 eV reversing the previous narrowing trend. This anomaly suggests the onset of more complex dopant-host interactions at higher doping levels. Several mechanisms such as Er–Er interactions may begin to dominate, leading to band splitting or the repulsion of impurity levels from the conduction band, also Local strain effects due to the larger Er^{3+} ionic radius of 2.45 Å and 1.46 Å for Si^{4+} could modify the electronic environment and the hybridization dynamics between Er 4f and O 2p orbitals may evolve with concentration, redistributing electronic density and pushing the CBM upward. This trend mirrors behaviors observed in other rare-earth doped systems [20, 23, 24], where the electronic effects of dopants are non-linear and concentration-dependent.

The band structure evolution with increasing Er concentration demonstrates that dopant level tuning enables control over the electronic nature of SiO_2, from indirect to direct band gap and from narrowed to expanded band widths. These results suggest a delicate balance between dopant-induced defect states, hybridization, and lattice effects, which play a critical role in tailoring SiO_2 for photonic, optoelectronic, and up conversion-based applications. The non-monotonic behavior at higher doping levels highlights the importance of optimizing Er concentration to achieve the desired performance without compromising structural or electronic integrity.

Table 4 illustrates the summary of the Er concentration trends.

Table 4. Summary of the Er concentration trends

Er Concentration	Doping Formula	Band Gap (eV)	Band Gap Type	Key Observation
0%	Pure SiO_2	5.32	Indirect	Wide, pristine semiconductor gap
2.08%	$Si_{0.9717}Er_{0.0283}O_2$	5.01	Direct	Gap narrowing due to impurity states
4.17%	$Si_{0.9583}Er_{0.0417}O_2$	5.08	Direct	Hybridization-driven band edge reshaping
6.25%	$Si_{0.9375}Er_{0.0625}O_2$	5.89	Direct	Gap widening due to complex dopant effects

3.3. *Effect of Interstitial Defects (OV and SiV) on the Electronic Properties of SiO_2*

In Figure 5 (a), the incorporation of an oxygen vacancy significantly alters the band structure of SiO_2 by reducing the band gap compared to pristine SiO_2 and introducing a deep donor level inside the band gap, just below the conduction band minimum (CBM). This donor level emerges due to the missing oxygen atom, which leaves behind two unpaired electrons. The associated localized positive charge creates an attractive potential that pulls nearby conduction band states down into the forbidden energy region. As a result, electronic states intrude into the gap from the conduction band, decreasing the effective band gap and making the material more conductive. This shift suggests that OV defects could act as electron donors and contribute to n-type conductivity in SiO_2, which may influence its dielectric breakdown strength and electrical leakage behavior in devices. Figure 5(b) shows that the silicon vacancy also causes a band gap reduction, but the nature of the changes is more complex than with the OV defect. The band gap becomes narrower, indicating increased electronic activity and, more importantly, the band gap undergoes a transition from indirect to direct band gap. This transformation is evidenced by a change in the curvature and alignment of the conduction and valence bands near the Fermi level. The conduction band minimum (CBM) and valence band maximum (VBM) aligning at the same k-point in reciprocal space, enabling direct electronic transitions. This direct band gap behavior implies that SiV defects enhance the optical absorption and emission potential of SiO_2, making such defect-engineered materials promising for photonic or light-emitting applications. Moreover, the modification in band curvature near the CBM implies a reduction in the effective mass of electrons, which may improve carrier mobility and influence transport properties. Table 5 shows the comparison and implications of the defect type.

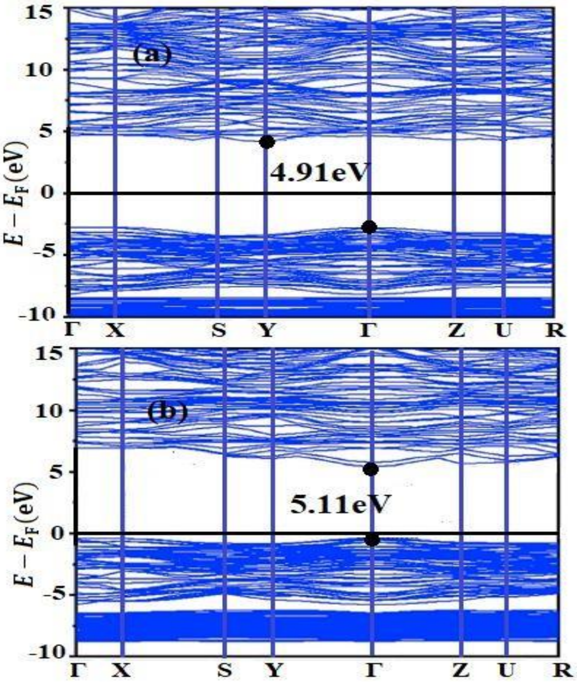

Fig. 5. Calculated band structures of (a) SiO_2 +OV and (b) SiO_2+SiV

Table 5. Comparison and implications of the defect type

Defect Type	Band Gap Effect	Nature of Change	Electronic Implication
Oxygen Vacancy (OV)	Band gap decreases significantly	Introduction of deep donor level	Potential n-type behavior, defect-related conductivity
Silicon Vacancy (SiV)	Band gap decreases moderately	Transition from indirect to direct gap	Enhanced optical activity, potential for light emission

3.4. Electronic Structure Evolution of Total and Projected Density of States (TDOS and PDOS) of SiO_2 with Er Doping

The total and projected density of states (TDOS and PDOS) calculations were performed for both pure and Er-doped SiO_2 systems, as illustrated in Figure 6(a-d). These plots reveal how different atomic orbitals contribute to the valence and conduction bands and provide insight into how Er incorporation alters the electronic structure of the host material.

Figure 6a shows TDOS and PDOS of an undoped Pristine SiO_2, which reveal a clear electronic structure dominated by oxygen and silicon orbitals. The valence band 0 to -15.8 eV is divided into three distinct sub-bands such as 0 to -5.4 eV which is dominated by O 2p states, with minor contributions from Si 3p, indicating effective s–p hybridization and -5.4 to -8.5 eV which is mostly Si 3s, along with a small portion of O 2p states while -13.66 to -14.99 eV shows that the deeper valence region is primarily due to O 2s states, contributing to a narrow, isolated peak. The conduction band begins just above the Fermi level 0 eV and is primarily composed of Si 3s and O 2p states, consistent with the wide indirect band gap observed in Figure 5(a). This configuration reflects the stable and insulating nature of pure SiO_2.

Figure 6 (b), 6 (c), and 6 (d) show the evolution of the density of states as the Er concentration increases from 2.08% to 6.25%, corresponding to $Si_{0.9717}Er_{0.0283}O_2$, $Si_{0.9583}Er_{0.0417}O_2$, and $Si_{0.9375}Er_{0.0625}O_2$, respectively. Despite Er incorporation, the core electronic structure of SiO_2 remains largely unchanged. The Si 3s/3p and O 2p/2s orbitals continue to dominate their respective energy ranges, showing that the host matrix retains its fundamental bonding character.

The new states that appear near the bottom of the conduction band and top of the valence band, attributed to Er 4f orbitals. These localized states contribute to the reduction in the conduction band minimum (CBM), which narrows the overall band gap by introducing impurity levels just below the CBM and induces a transition from an indirect to direct band gap, as previously discussed in the band structure analysis in Figure 5. As Er concentration increases, Er 5d orbitals begin to hybridize with the conduction band, becoming visible in the higher energy regions, and the Er 5p orbitals also appear in both the lower and upper parts of the spectrum, suggesting more significant orbital interaction at higher concentrations. At 2.08% and 4.17% Er concentration, the 4f impurity levels cause the band gap narrowing, consistent with the transition to a direct gap. Also, at 6.25% Er concentration, despite the presence of more impurity states, the conduction band shifts slightly upwards again, widening the band gap.

This suggests dopant-dopant interaction, lattice strain, or reconfiguration of bonding environments that suppress the gap-narrowing effect at higher concentrations.

The TDOS and PDOS results confirm that Er doping alters SiO_2's electronic structure primarily by introducing localized Er 4f states, which reduce the band gap and modify its nature. At moderate doping levels, this yields favorable conditions for optoelectronic activity, particularly via direct electronic transitions. However, as doping increases, the system exhibits nonlinear behavior, with increased contributions from Er 5d and 5p states that reconfigure the conduction band and lead to partial re-widening of the band gap. This analysis underscores the tunability of SiO_2's electronic properties via controlled Er doping, making it a promising candidate for customized photonic and optoelectronic applications, including lasers, amplifiers, and up-conversion devices. The Summary of the Orbital Contributions and Band Gap Impact is shown in Table 6.

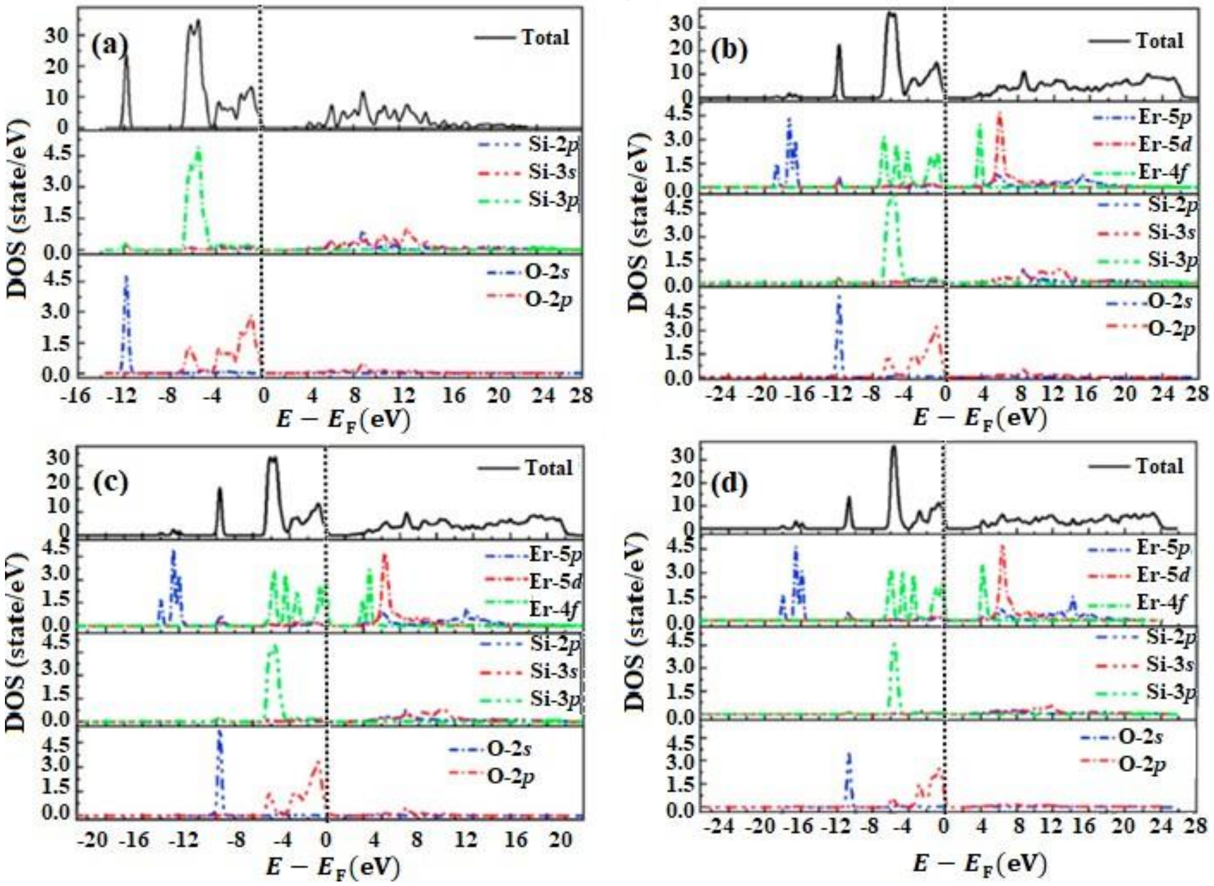

Fig. 6. Total and projected density of state of SiO_2 and SiO_2 doped systems, where the Fermi level is set to 0: (a) pure SiO_2, (b) $Si_{0.9717}Er_{0.0283}O_2$, (c) $Si_{0.9583}Er_{0.0417}O_2$, and (d) $Si_{0.9375}Er_{0.0625}O$

Table 6. Summary of Orbital Contributions and Band Gap Impact

Feature	Pure SiO_2	Low to Moderate Er Doping (2.08%–4.17%)	High Er Doping (6.25%)
Dominant VB States	O 2p, Si 3p	O 2p, Si 3p (unchanged)	O 2p, Si 3p
Dominant CB States	Si 3s, O 2p	Si 3s + Er 4f (impurity levels)	Si 3s + Er 4f, Er 5d
Impurity States Introduced	None	Er 4f near CBM and VBM	Er 4f, 5d, and 5p
Band Gap Trend	~5.32 eV (indirect)	↓ ~5.01–5.08 eV (direct)	↑ ~5.89 eV (direct)
Explanation	Stable host structure	Hybridization, sp-f interaction	Dopant interaction, strain

4. Conclusions

This study systematically investigates the structural, energetic, and electronic properties of erbium-doped silicon dioxide ($Er:SiO_2$) across concentrations of 2.08%, 4.17%, and 6.25%, alongside the effects of oxygen vacancies (OV) and silicon vacancies (SiV). In Structural and Thermodynamic Stability, Er^{3+} substitution induces lattice expansion, causes the cell volume to increase from 831.739 $Å^3$ in pure SiO_2 to 831.899 $Å^3$ at 6.25% Er, driven by the larger ionic radius of Er^{3+} at 2.45 Å and Si^{4+} at 1.46 Å, elongating Er–O bonds by 2.11 to 2.31 Å compared to Si–O bonds 1.61 Å. The Doped systems also exhibit enhanced thermodynamic stability, which shows evidenced by increasingly negative formation energies (Eform) from −0.552 eV/atom of pure SiO_2 to −0.724 eV/atom of (6.25%

Er), confirming favorable Er incorporation. The Er doping concentration of 2.08 and 4.17% narrows the bandgap to 5.01 and 5.08 eV from 5.32 eV in pure SiO_2 and induces an indirect-to-direct transition, facilitated by Er 4f-derived states near the conduction band minimum (CBM). At 6.25% Er, the bandgap unexpectedly widens to 5.89 eV due to emergent Er–Er interactions, lattice strain, and hybridization shifts, highlighting non-linear dopant-host dynamics. The OV introduce deep donor levels below the CBM, reducing the bandgap and promoting n-type conductivity, with lower formation energy of 1.76 eV/atom than SiVs while the SiV trigger a direct bandgap transition and enhance optoelectronic activity, despite higher formation energy of 1.97 eV/atom by modifying band curvature and reducing electron effective mass. The Charge Redistribution shows that the Mulliken charge analysis confirms charge compensation upon Er^{3+} substitution and Si atoms become more positive, from +1.28 to 1.38, while Er ions carry +1.58 to +1.62 charge, and oxygen atoms become less negative from −1.09 to −1.00, facilitating trivalent dopant integration. For the Technological Implications, the direct bandgap and tunable electronic transitions at 4.17% Er doping concentration optimize SiO_2 for fiber amplifiers and integrated photonics. The SiV induced direct gaps, which enable light-emitting devices, while OV mediated n-type behavior, which supports transparent electronics. Thermodynamic stability and defect-controlled band position Er and SiO_2 as a versatile platform for quantum technologies and up conversion systems.

Acknowledgements

The author would like to thank all related parties who helped with the process of this research, especially the Department of Physics, Kaduna State University Computational Lab, under the supervision of Dr Alhassan Shuaibu, where most of the calculations were carried out.

Funding Statement

This research received no specific grant from any funding agency.

Conflicts of interest

The authors declare that they have no known competing financial interests or personal relationships that could have appeared to influence the work reported in this paper.

Authors contribution statement

All authors contributed equally to this work.

References

[1] Azhagiri, S., Jayakumar, S., Gunasekaran, S., & Srinivasan, S. (2014). Molecular structure, Mulliken charge, frontier molecular orbital and first hyperpolarizability analysis on 2-nitroaniline and 4-methoxy-2-nitroaniline using density functional theory. *Spectrochimica Acta Part A: Molecular and Biomolecular Spectroscopy, 124*, 199-202.

[2] Akazawa, H. (2022). Er3+-catalyzed interdiffusion of elements across the interface between Bi2O3 film and SiO2 substrate resulting in host-material-specific photoluminescence spectra of Er3+. *Journal of Alloys and Compounds*, *904*, 164039.

[3] Beeler, B., Mahbuba, K., Wang, Y., & Jokisaari, A. (2021). Determination of thermal expansion, defect formation energy, and defect-induced strain of α-U via ab initio molecular dynamics. Frontiers in Materials, 8, 661387.

[4] Dorokhina, A., 2022. Luminescent Fluoride Nanomaterials Activated by Rare-Earth Ions.

[5] Fletcher, R., 2000. Practical methods of optimization. John Wiley & Sons.

[6] Giannozzi, P., 2020. Baseggio O. Bonfà P. Brunato D. Car R. Carnimeo I. Cavazzoni C. De Gironcoli S. Delugas P. Ferrari Ruffino F. et al. J. Chem. Phys, 152(154105), pp.10-1063.

[7] Fujiwara, T. and Hoshi, T., 1997. Optimized ultrasoft pseudopotentials. Journal of the Physical Society of Japan, 66(6), pp.1723-1729.

[8] Güler, E.M.R.E., Uğur, G.Ö.K.A.Y., Uğur, Ş.U.L.E. and Güler, M.E.L.E.K., 2020. A theoretical study for the band gap energies of the most common silica polymorphs. Chinese Journal of Physics, 65, pp.472-480.

[9] Henderson, G.S. and Stebbins, J.F., 2022. The short-range order (SRO) and structure. Reviews in Mineralogy and Geochemistry, 87(1), pp.1-53.

[10] Hohenberg, P. and Kohn, W.J.P.R., 1964. Density functional theory (DFT). Phys. Rev, 136(1964), p.B864.

[11] Hernández, E.V., Montufar, C.E.C., Ramírez, M.Á.C. and Hernández, F.M., 2024, February. Photoluminescence of Erbium-Doped ZnO Nanostructures. In Materials Science Forum (Vol. 1112, pp. 139-144). Trans Tech Publications Ltd.

[12] Jain, A., Ong, S.P., Hautier, G., Chen, W., Richards, W.D., Dacek, S., Cholia, S., Gunter, D., Skinner, D., Ceder, G. and Persson, K.A., 2013. Commentary: The Materials Project: A materials genome approach to accelerating materials innovation. APL materials, 1(1).

[13] Jain, A., Ong, S.P., Hautier, G., Chen, W., Richards, W.D., Dacek, S., Cholia, S., Gunter, D., Skinner, D., Ceder, G. and Persson, K.A., 2013. Commentary: The Materials Project: A materials genome approach to accelerating materials innovation. APL materials, 1(1).

[14] Larin, A.V. and Vercauteren, D.P., 1999. Approximation of Mulliken charges for the silicon atoms of all-siliceous zeolites. International Journal of Inorganic Materials, 1(3-4), pp.201-207.

[15] Peng, H. and Perdew, J.P., 2017. Rehabilitation of the Perdew-Burke-Ernzerhof generalized gradient approximation for layered materials. Physical Review B, 95(8), p.081105.

[16] Abdullah, A., Benchafia, E.M., Choi, D. and Abedrabbo, S., 2023. Synthesis and characterization of erbium-doped silica films obtained by an acid–base-catalyzed sol–gel process. Nanomaterials, 13(9), p.1508.

[17] Abedrabbo, S., Lahlouh, B., Fiory, A.T. and Ravindra, N.M., 2021. Optical polarizability of erbium-oxygen complexes in sol-gel-based silica films. Journal of Physics D: Applied Physics, 54(13), p.135101.

[18] Muy, S., Schlem, R., Shao-Horn, Y. and Zeier, W.G., 2021. Phonon–ion interactions: designing ion mobility based on lattice dynamics. Advanced Energy Materials, 11(15), p.2002787.

[19] Peng, H. and Perdew, J.P., 2017. Rehabilitation of the Perdew-Burke-Ernzerhof generalized gradient approximation for layered materials. Physical Review B, 95(8), p.081105.

[20] Tse, G., 2021. The electronic and optical properties of SiO2–Al–SiO2 with density functional theory. Modern physics letters B, 35(08), p.2150136.

[21] Wang, Q., Wen, J., Luo, Y., Peng, G.D., Pang, F., Chen, Z. and Wang, T., 2020. Enhancement of lifetime in Er-doped silica optical fiber by doping Yb ions via atomic layer deposition. Optical Materials Express, 10(2), pp.397-407.

[22] Wardani, D.A.P., Hariyanto, B., Kurniawati, N., Har, N.P., Darmawan, N. and Irzaman, I., 2023. Functional groups, band gap energy, and morphology properties of annealed silicon dioxide (SiO2). Egyptian Journal of Chemistry, 66(3), pp.529-535.

[23] Liu, G., Wang, F., Guan, X., Jia, B., Han, L., Yan, B., Peng, G.D. and Lu, P., 2020. Geometric and optical properties of Bi/Er co-doped silica optical fiber. Optical Materials, 107, p.110030.

[24] Yang, Y., Takahashi, M., Abe, H. and Kawazoe, Y., 2008. Structural, electronic and optical properties of the Al2O3 doped SiO2: first principles calculations. Materials transactions, 49(11), pp.2474-2479.